EUROPEAN ORGANIZATION FOR NUCLEAR RESEARCH

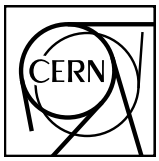

CERN-EP-2020-041
24 March 2020

Antiproton over proton and K^- over K^+ multiplicity ratios at high z in DIS

The COMPASS Collaboration

Abstract

The $\bar{p}$ over p multiplicity ratio is measured in deep-inelastic scattering for the first time using (anti-) protons carrying a large fraction of the virtual-photon energy, $z > 0.5$. The data were obtained by the COMPASS Collaboration using a 160 GeV muon beam impinging on an isoscalar ^{6}LiD target. The regime of deep-inelastic scattering is ensured by requiring $Q^2 > 1$ (GeV/c)^2 for the photon virtuality and $W > 5$ GeV/c^2 for the invariant mass of the produced hadronic system. The range in Bjorken-x is restricted to $0.01 < x < 0.40$. Protons and antiprotons are identified in the momentum range $20 \div 60$ GeV/c. In the whole studied z-region, the $\bar{p}$ over p multiplicity ratio is found to be below the lower limit expected from calculations based on leading-order perturbative Quantum Chromodynamics (pQCD). Extending our earlier analysis of the K^- over K^+ multiplicity ratio by including now events with larger virtual-photon energies, this ratio becomes closer to the expectation of next-to-leading order pQCD. The results of both analyses strengthen our earlier conclusion that the phase space available for hadronisation should be taken into account in the pQCD formalism.

(to be submitted to PLB)

The COMPASS Collaboration

M.G. Alexeev[25,26], G.D. Alexeev[7], A. Amoroso[25,26], V. Andrieux[9,28], V. Anosov[7], A. Antoshkin[7], K. Augsten[7,18], W. Augustyniak[29], C.D.R. Azevedo[1], B. Badełek[30], F. Balestra[25,26], M. Ball[3], J. Barth[3], R. Beck[3], Y. Bedfer[20], J. Berenguer Antequera[25,26], J. Bernhard[12,9], M. Bodlak[17], F. Bradamante[24], A. Bressan[23,24], M. Büchele[8], V. E. Burtsev[27], W.-C. Chang[21], C. Chatterjee[23,24], M. Chiosso[25,26], A. G. Chumakov[27], S.-U. Chung[15,a,b] A. Cicuttin[24,c] P. M. M. Correia[1], M.L. Crespo[24,c], D. D'Ago[23,24], S. Dalla Torre[24], S.S. Dasgupta[6], S. Dasgupta[24], I. Denisenko[7], O.Yu. Denisov[26,#], , S.V. Donskov[19], N. Doshita[32], Ch. Dreisbach[15], W. Dünnweber[d], R. R. Dusaev[27], A. Efremov[7], P.D. Eversheim[3], P. Faccioli[11], M. Faessler[d], M. Finger[17], M. Finger jr.[17], H. Fischer[8], C. Franco[11], J.M. Friedrich[15], V. Frolov[7,9], F. Gautheron[2,28], O.P. Gavrichtchouk[7], S. Gerassimov[14,15], J. Giarra[12], I. Gnesi[25,26], M. Gorzellik[8,e], A. Grasso[25,26], A. Gridin[7], M. Grosse Perdekamp[28], B. Grube[15], A. Guskov[7], D. von Harrach[12], R. Heitz[28], F. Herrmann[8], N. Horikawa[16,f], N. d'Hose[20], C.-Y. Hsieh[21,g], S. Huber[15], S. Ishimoto[32,h], A. Ivanov[7], T. Iwata[32], M. Jandek[18], V. Jary[18], R. Joosten[3], P. Jörg[8,i], E. Kabuß[12], F. Kaspar[15], A. Kerbizi[23,24], B. Ketzer[3], G.V. Khaustov[19], Yu.A. Khokhlov[19,j],Yu. Kisselev[7], F. Klein[4], J.H. Koivuniemi[2,28], V.N. Kolosov[19], K. Kondo Horikawa[32], I. Konorov[14,15], V.F. Konstantinov[19], A.M. Kotzinian[26,k], O.M. Kouznetsov[7], A. Koval[29], Z. Kral[17], F. Krinner[15], Y. Kulinich[28], F. Kunne[20], K. Kurek[29], R.P. Kurjata[31], A. Kveton[17], K. Lavickova[17], S. Levorato[24], Y.-S. Lian[21,l], J. Lichtenstadt[22], P.-J. Lin[20,m], R. Longo[28], V. E. Lyubovitskij[27,n], A. Maggiora[26], A. Magnon[o], N. Makins[28], N. Makke[24,c], G.K. Mallot[9,8], A. Maltsev[7], S. A. Mamon[27], B. Marianski[29], A. Martin[23,24], J. Marzec[31], J. Matoušek[23,24], T. Matsuda[13], G. Mattson[28], G.V. Meshcheryakov[7], M. Meyer[28,20], W. Meyer[2], Yu.V. Mikhailov[19], M. Mikhasenko[3,9], E. Mitrofanov[7], N. Mitrofanov[7], Y. Miyachi[32], A. Moretti[23,24], A. Nagaytsev[7], C. Naim[20], D. Neyret[20], J. Nový[18], W.-D. Nowak[12], G. Nukazuka[32], A.S. Nunes[11,p], A.G. Olshevsky[7], M. Ostrick[12], D. Panzieri[26,q], B. Parsamyan[25,26], S. Paul[15], H. Pekeler[3], J.-C. Peng[28], M. Pešek[17], D.V. Peshekhonov[7], M. Pešková[17], N. Pierre[12,20], S. Platchkov[20], J. Pochodzalla[12], V.A. Polyakov[19], J. Pretz[4,s], M. Quaresma[21,11], C. Quintans[11], G. Reicherz[2], C. Riedl[28], T. Rudnicki[30], D.I. Ryabchikov[19,15], A. Rybnikov[7], A. Rychter[31], V.D. Samoylenko[19], A. Sandacz[29], S. Sarkar[6], I.A. Savin[7], G. Sbrizzai[23,24], H. Schmieden[4], A. Selyunin[7], L. Sinha[6], M. Slunecka[7,17], J. Smolik[7], A. Srnka[5], D. Steffen[9,15], M. Stolarski[11,#], , O. Subrt[9,18], M. Sulc[10], H. Suzuki[32,f], P. Sznajder[29], S. Tessaro[24], F. Tessarotto[24,9,#], , A. Thiel[3], J. Tomsa[17], F. Tosello[26], A. Townsend[28], V. Tskhay[14], S. Uhl[15], B. I. Vasilishin[27], A. Vauth[4,9,r], B. M. Veit[12,9], J. Veloso[1], B. Ventura[20], A. Vidon[20], M. Virius[18], M. Wagner[3], S. Wallner[15], K. Zaremba[31], P. Zavada[7], M. Zavertyaev[14], M. Zemko[17], E. Zemlyanichkina[7], Y. Zhao[24] and M. Ziembicki[31]

[1] University of Aveiro, Dept. of Physics, 3810-193 Aveiro, Portugal
[2] Universität Bochum, Institut für Experimentalphysik, 44780 Bochum, Germany[t,u]
[3] Universität Bonn, Helmholtz-Institut für Strahlen- und Kernphysik, 53115 Bonn, Germany[t]
[4] Universität Bonn, Physikalisches Institut, 53115 Bonn, Germany[t]
[5] Institute of Scientific Instruments of the CAS, 61264 Brno, Czech Republic[v]
[6] Matrivani Institute of Experimental Research & Education, Calcutta-700 030, India[w]
[7] Joint Institute for Nuclear Research, 141980 Dubna, Moscow region, Russia[x]
[8] Universität Freiburg, Physikalisches Institut, 79104 Freiburg, Germany[t,u]
[9] CERN, 1211 Geneva 23, Switzerland
[10] Technical University in Liberec, 46117 Liberec, Czech Republic[v]
[11] LIP, 1649-003 Lisbon, Portugal[y]
[12] Universität Mainz, Institut für Kernphysik, 55099 Mainz, Germany[t]
[13] University of Miyazaki, Miyazaki 889-2192, Japan[z]
[14] Lebedev Physical Institute, 119991 Moscow, Russia
[15] Technische Universität München, Physik Dept., 85748 Garching, Germany[t,d]
[16] Nagoya University, 464 Nagoya, Japan[z]

[17] Charles University, Faculty of Mathematics and Physics, 12116 Prague, Czech Republic[v]
[18] Czech Technical University in Prague, 16636 Prague, Czech Republic[v]
[19] State Scientific Center Institute for High Energy Physics of National Research Center 'Kurchatov Institute', 142281 Protvino, Russia
[20] IRFU, CEA, Université Paris-Saclay, 91191 Gif-sur-Yvette, France[u]
[21] Academia Sinica, Institute of Physics, Taipei 11529, Taiwan[aa]
[22] Tel Aviv University, School of Physics and Astronomy, 69978 Tel Aviv, Israel[ab]
[23] University of Trieste, Dept. of Physics, 34127 Trieste, Italy
[24] Trieste Section of INFN, 34127 Trieste, Italy
[25] University of Turin, Dept. of Physics, 10125 Turin, Italy
[26] Torino Section of INFN, 10125 Turin, Italy
[27] Tomsk Polytechnic University, 634050 Tomsk, Russia[ac]
[28] University of Illinois at Urbana-Champaign, Dept. of Physics, Urbana, IL 61801-3080, USA[ad]
[29] National Centre for Nuclear Research, 02-093 Warsaw, Poland[ae]
[30] University of Warsaw, Faculty of Physics, 02-093 Warsaw, Poland[ae]
[31] Warsaw University of Technology, Institute of Radioelectronics, 00-665 Warsaw, Poland[ae]
[32] Yamagata University, Yamagata 992-8510, Japan[z]

[#] Corresponding authors
[a] Also at Dept. of Physics, Pusan National University, Busan 609-735, Republic of Korea
[b] Also at Physics Dept., Brookhaven National Laboratory, Upton, NY 11973, USA
[c] Also at Abdus Salam ICTP, 34151 Trieste, Italy
[d] Supported by the DFG cluster of excellence 'Origin and Structure of the Universe' (www.universe-cluster.de) (Germany)
[e] Supported by the DFG Research Training Group Programmes 1102 and 2044 (Germany)
[f] Also at Chubu University, Kasugai, Aichi 487-8501, Japan
[g] Also at Dept. of Physics, National Central University, 300 Jhongda Road, Jhongli 32001, Taiwan
[h] Also at KEK, 1-1 Oho, Tsukuba, Ibaraki 305-0801, Japan
[i] Present address: Universität Bonn, Physikalisches Institut, 53115 Bonn, Germany
[j] Also at Moscow Institute of Physics and Technology, Moscow Region, 141700, Russia
[k] Also at Yerevan Physics Institute, Alikhanian Br. Street, Yerevan, Armenia, 0036
[l] Also at Dept. of Physics, National Kaohsiung Normal University, Kaohsiung County 824, Taiwan
[m] Supported by ANR, France with P2IO LabEx (ANR-10-LBX-0038) in the framework "Investissements d'Avenir" (ANR-11-IDEX-003-01)
[n] Also at Institut für Theoretische Physik, Universität Tübingen, 72076 Tübingen, Germany
[o] Retired
[p] Present address: Brookhaven National Laboratory, Brookhaven, USA
[q] Also at University of Eastern Piedmont, 15100 Alessandria, Italy
[r] Present address: Universität Hamburg, 20146 Hamburg, Germany
[s] Present address: RWTH Aachen University, III. Physikalisches Institut, 52056 Aachen, Germany
[t] Supported by BMBF - Bundesministerium für Bildung und Forschung (Germany)
[u] Supported by FP7, HadronPhysics3, Grant 283286 (European Union)
[v] Supported by MEYS, Grant LM20150581 (Czech Republic)
[w] Supported by B. Sen fund (India)
[x] Supported by CERN-RFBR Grant 12-02-91500
[y] Supported by FCT, Grants CERN/FIS-PAR/0007/2017 and CERN/FIS-PAR/0022/2019 (Portugal)
[z] Supported by MEXT and JSPS, Grants 18002006, 20540299, 18540281 and 26247032, the Daiko and Yamada Foundations (Japan)
[aa] Supported by the Ministry of Science and Technology (Taiwan)
[ab] Supported by the Israel Academy of Sciences and Humanities (Israel)

[ac] Supported by the Russian Federation program “Nauka” (Contract No. 0.1764.GZB.2017) (Russia)
[ad] Supported by the National Science Foundation, Grant no. PHY-1506416 (USA)
[ae] Supported by NCN, Grant 2017/26/M/ST2/00498 (Poland)

1 Introduction

Within the standard approach of perturbative Quantum Chromodynamics (pQCD), hadron production from an active quark in a deep-inelastic scattering process (DIS) is effectively described by non-perturbative objects called fragmentation functions (FFs). These functions presently cannot be predicted by theory, but their scale evolution is described by the DGLAP equations [1]. For a given negative four-momentum transfer squared Q^2, in leading order (LO) pQCD the FF $D_q^h(z,Q^2)$ represents the probability density that a hadron h is produced in the fragmentation of a quark with flavour q. The produced hadron carries a fraction z of the virtual-photon energy ν, where the latter is defined in the laboratory frame.

The cleanest way to access FFs consists in studying single-inclusive hadron production in lepton annihilation, $e^+ + e^- \to h+X$, where the remaining final state X is not analysed. However, only information about $D_q^h + D_{\bar{q}}^h$ is accessible there and only limited flavour separation is possible. Additional input, like semi-inclusive measurements of deep-inelastic lepton-nucleon scattering (SIDIS), is required to fully understand quark fragmentation into hadrons. In the case of the SIDIS cross section, fragmentation functions are convoluted with parton distribution functions (PDFs). As these are rather well known, fragmentation functions for q and $\bar{q}$ can be accessed separately and full flavour separation is possible in principle. As a result, fragmentation functions obtained using only e^+e^- data differ in some cases significantly from those that were determined by additionally taking into account data from SIDIS or other processes, see Refs. [2–7].

Recently, the HERMES and COMPASS Collaborations have published several papers concerning unidentified hadron, pion and kaon multiplicities in SIDIS, see Refs. [8–11]. In the most recent COMPASS article [12] it was shown that for kaons at high z the K^- over K^+ multiplicity ratio R_K falls below the lower limit predicted by pQCD. From the measured ν-dependence it was concluded that in experiments with similar or lower centre-of-mass energy than in COMPASS an insufficient description of the data by pQCD may affect the high-z region. This kinematic region is important in many respects, as *e.g.* transverse-momentum-dependent azimuthal asymmetries are quite pronounced there [13]. Hence the above described phenomenon should be better understood in order to avoid possible bias when extracting fragmentation functions and/or transverse-momentum-dependent PDFs and FFs by applying the naive pQCD formalism to SIDIS data in the high-z region.

In order to provide more experimental input for further phenomenological studies, we present here for the first time the COMPASS results on the $\bar{p}$ over p multiplicity ratio R_p at high z, *i.e.* $z > 0.5$, which are obtained from SIDIS data taken on an isoscalar target. In addition we present new results on R_K, obtained in a ν-range extended with respect to Ref. [12], which became attainable by improving the kaon identification procedure. Note that when measuring a multiplicity ratio, several systematic uncertainties cancel in both theory and experiment. Thus a multiplicity ratio can be considered as one of the most robust observables presently available when analysing SIDIS data.

This Letter is organised as follows. In Section 2, pQCD-based predictions for R_p and R_K are discussed. Experimental set-up and data selection are described in Section 3. The analysis method is presented in Section 4, followed by the discussion of systematic uncertainties in Section 5. The results are presented and discussed in Section 6.

2 Theoretical framework and model expectations

Hadrons of type h produced in the final state of DIS are commonly characterised by their relative abundance. The hadron multiplicity M^h is defined as ratio of the SIDIS cross section for hadron type h and the cross section for an inclusive measurement of the deep-inelastic scattering process (DIS):

$$\frac{dM^h(x,Q^2,z)}{dz} = \frac{d^3\sigma^h(x,Q^2,z)/dx dQ^2 dz}{d^2\sigma^{DIS}(x,Q^2)/dx dQ^2}. \quad (1)$$

Here, x denotes the Bjorken scaling variable. The cross sections σ^{DIS} and σ^{h} can be composed using the standard factorisation approach of pQCD [14, 15]. In the following, the LO pQCD expressions for the cross section calculations will be used. In the LO approximation for the multiplicity, where the sum over parton species $a = \mathrm{q}, \bar{\mathrm{q}}$ is weighted by the square of the electric charge e_a of the quark expressed in units of the elementary charge, only simple products of PDFs $f_a(x, Q^2)$ and FFs $D_a^{\mathrm{h}}(z, Q^2)$ are involved instead of the aforementioned convolutions:

$$\frac{\mathrm{d}M^{\mathrm{h}}(x, Q^2, z)}{\mathrm{d}z} = \frac{\sum_a e_a^2 f_a(x, Q^2) D_a^{\mathrm{h}}(z, Q^2)}{\sum_a e_a^2 f_a(x, Q^2)}. \tag{2}$$

For a deuteron target, the $\bar{\mathrm{p}}$ over p multiplicity ratio in LO pQCD reads as follows:

$$R_{\mathrm{p}}(x, Q^2, z) = \frac{\mathrm{d}M^{\bar{\mathrm{p}}}(x, Q^2, z)/\mathrm{d}z}{\mathrm{d}M^{\mathrm{p}}(x, Q^2, z)/\mathrm{d}z} = \frac{4.5(\bar{\mathrm{u}} + \bar{\mathrm{d}})D_{\mathrm{fav}} + (5\mathrm{u} + 5\mathrm{d} + 2\mathrm{s} + 2\bar{\mathrm{s}})D_{\mathrm{unf}}}{4.5(\mathrm{u} + \mathrm{d})D_{\mathrm{fav}} + (5\bar{\mathrm{u}} + 5\bar{\mathrm{d}} + 2\mathrm{s} + 2\bar{\mathrm{s}})D_{\mathrm{unf}}}. \tag{3}$$

Here, u, $\bar{\mathrm{u}}$, d, $\bar{\mathrm{d}}$, s, $\bar{\mathrm{s}}$ denote the PDFs in the proton for corresponding quark flavours. Their dependences on x and Q^2 are omitted for brevity. The symbols D_{fav} (D_{unf}) denote favoured (unfavoured) fragmentation functions and their dependence on z and Q^2 are also omitted for brevity. Presently, proton FFs and their ratios are not well known at high z as their extraction is based on $\mathrm{e^+e^-}$ annihilation data only [2]. Following Refs. [2] and [16] it is assumed that $D_{\mathrm{u}}^{\mathrm{p}} = 2D_{\mathrm{d}}^{\mathrm{p}} = D_{\mathrm{fav}}$. In addition, the existing data do not allow to distinguish between different functions D_{unf} for different quark flavours. In the large-z region, the ratios $D_{\mathrm{unf}}/D_{\mathrm{fav}}$ are expected to be small [1]. Neglecting D_{unf} in Eq. (3) leads to the following lower limit for R_{p} in LO pQCD

$$R_{\mathrm{p}} > \frac{\bar{\mathrm{u}} + \bar{\mathrm{d}}}{\mathrm{u} + \mathrm{d}}, \tag{4}$$

which depends only upon rather well known PDFs, and is independent on the assumption that $D_{\mathrm{u}}^{\mathrm{p}} = 2D_{\mathrm{d}}^{\mathrm{p}} = D_{\mathrm{fav}}$. It is interesting to notice that the value of the lower limit predicted by LO pQCD is the same for both protons and kaons, see Ref. [12]. However, one expects $R_{\mathrm{K}} > R_{\mathrm{p}}$ as in the case of kaons the strange quark FFs ($D_{\mathrm{s}}^{\mathrm{K}^-}, D_{\bar{\mathrm{s}}}^{\mathrm{K}^+}$) are of the favoured type, contrary to the proton case. The expected value of $R_{\mathrm{K}}/R_{\mathrm{p}}$ is about 1.10 when using FFs from Ref. [5] and the MSTW08LO PDF set from Ref. [17], where the strange-quark contribution is suppressed with respect to the light-quark sea. It can be as large as 1.15 if strange quarks are not suppressed with respect to the light-quark sea as suggested by the interpretation of some LHC measurements [18, 19]. On the other hand, newer kaon FFs that are available only at NLO [6] suggest that the ratio of $D_{\bar{\mathrm{s}}}^{K^+}/D_{\mathrm{u}}^{K^+}$ is about 1.5 times smaller than originally obtained in Ref. [5]. In this case, $R_{\mathrm{K}}/R_{\mathrm{p}}$ is reduced back to about 1.10. Therefore, $R_{\mathrm{K}}/R_{\mathrm{p}} = 1.10 \pm 0.05$ appears as a reasonable expectation based on the LO pQCD formalism.

The present analysis is performed in two x-bins, below and above $x = 0.05$. The average values of x and Q^2 are $\langle x \rangle = 0.023$, $\langle Q^2 \rangle$ = 2.4 (GeV/c)^2 in the first x-bin and $\langle x \rangle = 0.10$, $\langle Q^2 \rangle$ = 9.8 (GeV/c)^2 in the second one. Based on Eq. (4) and the MSTW08LO PDF set, the expected lower limits on R_{p} in these two x-bins are 0.51 and 0.28. These values are about 10% higher if newer PDF sets as in Refs. [18, 19] are used instead. Due to the above mentioned lack of reliable proton FFs at NLO, presently no predictions can be made for the lower limit of R_{p} at higher perturbative order.

We also evaluate R_{p} with the LEPTO Monte Carlo event generator [20] (version 6.5), with the result that the LUND string fragmentation model [21] used in LEPTO is incapable to model R_{p} correctly. For example, for $z \approx 0.5$ LEPTO predicts $R_{\mathrm{p}} \approx 1$, which is definitely not supported by the data as it will be shown below. On the other hand, for $z > 0.85$ the predicted value of R_{p} falls below the naive LO pQCD lower limit. This is possible as in the LUND model the mechanism of string hadronisation does not only

[1] For kaons, this expectation is indeed confirmed in pQCD fits already at moderate values of z, see *e.g.* Ref. [6].

depend on quark and hadron types and on z, as in the pQCD formalism, but also on the type of the target nucleon and on x, see Ref. [22] for more details.

Due to different lower momentum limits for particle identification at COMPASS, 18 GeV/c for protons and 9 GeV/c for kaons, the observed x and Q^2 distributions are slightly different for pions and kaons. As a result, the lower limit on R_{K} is about 0.47, which is obtained for $\langle x \rangle = 0.03$ and $\langle Q^2 \rangle$ = 1.6 (GeV/c)^2. The LO pQCD predictions for the lower limit on R_{K} are ν independent, because they depend on PDFs in the same way as given in Eq. (4) for the proton case. However, in our earlier measurement [12] a clear ν dependence was observed. With higher values of ν accessible in the current measurement, we expect the results to be in better agreement with the expectation of (N)LO pQCD. We also note that the NLO lower limit for R_{K} turns out to be $10 \div 15\%$ smaller than the LO pQCD lower limit given above, see Ref. [12].

Some phenomenological models [23–25] are able to accommodate R_{K} below the pQCD limits presented above, but the predicted effect is too small to explain our earlier published results [12]. There are also important theoretical efforts ongoing to improve the formalism (higher-order corrections, treatment of heavy quarks *etc.*), see *e.g.* Refs. [26–31], which however do not affect the interpretation of the data shown in Ref. [12] and in the present paper.

3 Experimental set-up and data selection

The present analysis is based on COMPASS data taken in 2006. The 160 GeV/c μ^+ beam delivered by the M2 beam line of the CERN SPS had a momentum spread of about 5%. The beam was naturally polarised, but the polarisation is not affecting this analysis since we integrate over azimuthal angle and transverse momentum of the produced hadrons. The ^{6}LiD target has a total length of 120 cm, which corresponds to about half of a hadron interaction length. It is considered to be isoscalar, and the 0.2% excess of neutrons over protons due to the presence of additional material in the target (^{3}He and ^{7}Li) is neglected. The target was longitudinally polarised, but in the present analysis the data are averaged over the target polarisation, which leads to a remaining average target polarisation below 1%.

The COMPASS two-stage spectrometer has a polar-angle acceptance of $\pm$180 mrad, and it is capable of detecting charged particles with momenta as low as 0.5 GeV/c. However, in this analysis typical particle momenta are above 20 GeV/c. The ring-imaging Cherenkov detector (RICH) was used to identify pions, kaons and protons. Its radiator volume was filled with C_4F_{10} leading to a threshold for pion, kaon and proton identification of about 3 GeV/c, 9 GeV/c and 18 GeV/c respectively. Two trigger types are used in the analysis. The "inclusive" trigger is based on a signal from a combination of hodoscope signals caused by the scattered muon. The "semi-inclusive" trigger requires an energy deposition in one of the hadron calorimeters. The experimental set-up is described in more detail in Ref. [32].

The data selection criteria are kept similar to those used in the recently published analyses [10, 12] whenever possible. In order to formally ensure the applicability of the pQCD formalism, the DIS region is selected by requiring $Q^2 > 1$ (GeV/c)^2 and $W > 5$ GeV/c^2 for the invariant mass of the produced hadronic system. The fraction of the incoming muon energy carried by the virtual photon, y, is kept larger than 0.1 to avoid the region with degraded momentum resolution.

For the proton multiplicity analysis, the constraint $x > 0.01$ is used in order to make the kinematic coverage more similar to that of our earlier kaon studies [12]. In the present analysis, we study protons carrying a large fraction z of the virtual-photon energy, $z > 0.5$. In order to ensure efficient proton identification by the RICH, only events with proton momentum above 20 GeV/c are used, *i.e.* 2 GeV/c above the RICH proton threshold. The upper limit for proton identification is set to 60 GeV/c. Purity and efficiency of the proton selection are optimised by imposing appropriate constraints on the likelihoods of proton, kaon, pion and background hypotheses that are calculated by the RICH particle-identification software [33].

In our earlier studies of $R_{\rm K}$ [12], kaons with momenta between 12 GeV/c and 40 GeV/c were analysed for $z > 0.75$. By the improvements in the RICH particle-identification software described in Section 4, the momentum range extends now up to 55 GeV/c, which leads to a significant extension of the available ν range. All other kaon selection criteria remain unchanged with respect to the earlier analysis.

4 Analysis method

The proton (kaon) multiplicities $M^{\rm p(K)}(x, Q^2, z)$ are determined from the proton (kaon) yields $N^{\rm p(K)}$ normalised by the number of DIS events, $N^{\rm DIS}$, and corrected by the acceptance $A^{\rm p(K)}(x,Q^2,z)$:

$$\frac{{\rm d}M^{\rm p(K)}(x,Q^2,z)}{{\rm d}z} = \frac{1}{N^{\rm DIS}(x,Q^2)} \frac{{\rm d}N^{\rm p(K)}(x,Q^2,z)}{{\rm d}z} \frac{1}{A^{\rm p(K)}(x,Q^2,z)}\,. \tag{5}$$

As in our earlier kaon analysis [12], we use "semi-inclusive" triggers. This is possible because a bias-free determination of $N^{\rm DIS}$ is not needed, as the latter cancels in $R_{\rm p}$ and $R_{\rm K}$. The total number of protons and anti-protons used in the analysis is about 50 000. In addition to about 64 000 kaons analysed in Ref. [12], there are about 13 000 kaons more in the newly explored kinematic range. Note that the kinematic range for protons is wider than that for kaons.

As it was mentioned in Section 2, the proton analysis is performed in two x-bins, below and above $x = 0.05$. In each x-bin, nine bins are used in the reconstructed z variable $z_{\rm rec}$, with the bin limits 0.50, 0.55, 0.60, 0.65, 0.70, 0.75, 0.80, 0.85, 0.90 and 1.10. In addition, for events in the first x-bin the data are separated in four bins of proton momentum $p_{\rm h}$, with the bin limits 20 GeV/c, 30 GeV/c, 40 GeV/c, 50 GeV/c and 60 GeV/c. This 2-dimensional binning allows implicit studies of the ν-dependence of $R_{\rm p}$. For the second x-bin, the anti-proton statistics is too limited to perform the analysis in the additional dimension of (anti-)proton momentum. For kaons the present analysis is only performed for $x < 0.05$, using five z-bins with bin limits 0.75, 0.80, 0.85, 0.90, 0.95 and 1.05, and three momentum bins with bin limits 40 GeV/c, 45 GeV/c, 50 GeV/c and 55 GeV/c.

In order to determine the multiplicity ratio $R_{\rm p}$ from the raw yield of $\bar{\rm p}$ and p, only a few correction factors have to be taken into account. First, the correction related to RICH efficiencies is applied. From an analysis of Λ^0 and $\overline{\Lambda^0}$ decays into an (anti-)proton-pion pair it was concluded that the RICH efficiency for p is charge-symmetric within a precision of about 1%. The proton selection, which was improved with respect to our earlier papers, ensures that the contamination from π and K can be safely neglected. Upper limits to such a possible contamination are taken into account in the systematic uncertainty. The acceptance correction factors $A^{\rm p}$ for p and $\bar{\rm p}$ are determined using Monte Carlo simulations. The same unfolding method is used as in Ref. [12], *i.e.*, in a given (x, Q^2) bin we calculate the ratio of the number of reconstructed events to that of generated ones. Note that in order to count generated (reconstructed) events, generated (reconstructed) variables are used. As for z unfolding, we present the results as a function of z_{corr}, which denotes the value of z reconstructed in the experiment, corrected by the average difference between the generated and reconstructed values of z_{rec}, where the latter are determined by Monte Carlo simulations. The average acceptance ratio for the first x-bin is $A_{\bar{\rm p}}/A_{\rm p} = 0.912 \pm 0.004$ (stat.) and a similar value is obtained for the second x-bin. The systematic uncertainty related to the acceptance ratio is discussed in the next section. It is also verified by using the DJANGOH Monte Carlo generator [34] that in the COMPASS kinematics the radiative correction for positive and negative particles is of the same value within uncertainties, thus it cancels in the ratio.

Compared to the above proton analysis and the kaon analysis presented in Ref. [12], the raw $\rm K^{\pm}$ yields are obtained in a different way, which is described below. After that, the present analysis follows closely the same procedure as in the case of the proton analysis and the one from Ref. [12]. With respect to the proton analysis described above it is in addition verified using simulations that the contamination from diffractive vector meson decays (*e.g.* $\phi \to {\rm K^+K^-}$) and charm meson decays is negligible.

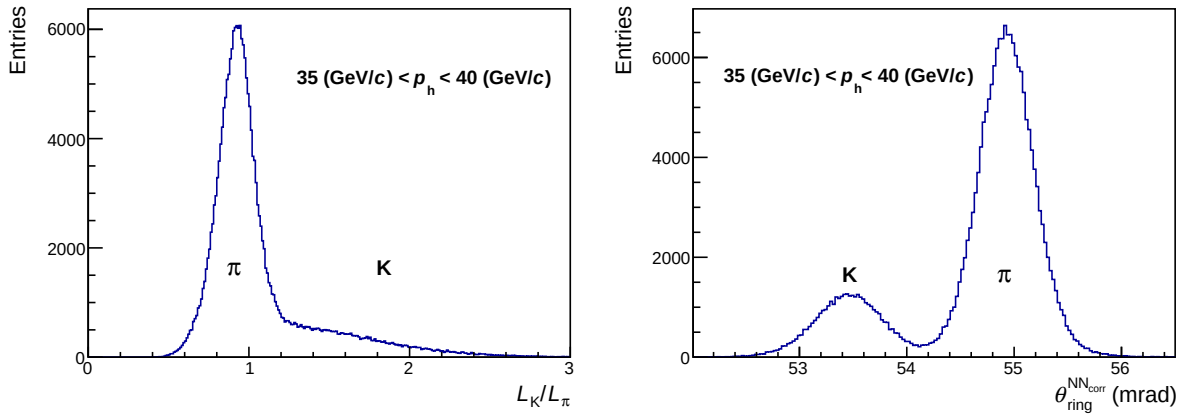

Fig. 1: Left panel: RICH likelihood ratio of K over π hypotheses for tracks with momenta between 35 GeV/c and 40 GeV/c where the separation between K and π is not obvious. In order to select kaons, the constraint $L_K/L_\pi > 1.5$ was used in Ref. [12]. Right panel: reconstructed angle of Cherenkov photons in the "ring fit" after the NN correction (which is used in the present analysis), for the same data as shown in the left panel. Here, a much cleaner separation between π and K is visible.

In the proton analysis and in the kaon analysis from Ref. [12], the raw yields are obtained directly by counting the number of events that fulfil certain criteria of RICH particle identification. However, by improving the RICH particle-identification software a better separation between π and K can be achieved at higher momenta. For the present analysis, the polar angle θ of the Cherenkov photon rings is corrected by a Neural Networks (NN) parametrisation, which intends to improve the internal description of the RICH sub-structure with respect to what was known during the original data production and the reconstruction. This correction depends upon various track parameters like position and angle at the RICH entrance, momentum of the particle *etc.* and is applied on an event-by-event basis. In the left panel of Fig. 1, we recall from our earlier analysis [12] the likelihood ratio for the K/π hypothesis in the highest momentum bin, where the separation was most challenging. In order to optimise the uncertainties of R_K, a lower limit of 1.5 had to be used there. Using in the present analysis the NN method, the separation of kaons and pions is improved considerably as illustrated in the right panel of Fig. 1, where the θ distribution after the NN correction is shown for the same events as in the left panel. A much better separation of the two particle species is clearly visible, which allows us to extend the analysis to higher momenta up to 55 GeV.

In order to obtain the raw kaon yield, the spectra as the one shown in the right panel of Fig. 1 are fitted in each z and p_h bin using the functional form described below. It turns out that a single Gaussian to describe the kaon peak and two Gaussians for the pion peak are sufficient to obtain the raw kaon yield. The fit is performed simultaneously in all z and p_h bins. This procedure is a source of non-negligible systematic uncertainties, especially at higher z and higher momenta. The systematic uncertainty related to this extraction is described in Section 5.

5 Studies of systematic uncertainties

This section is split into two parts. In the first part, studies of systematic effects for the proton results are described. This is a rather standard analysis that benefits from the significant knowledge acquired with the previously published COMPASS analyses [9, 10, 12]. In the second part, the kaon results are described. As for the first time in COMPASS a new method is used to estimate the kaon yield, detailed studies are performed to verify the reliability of the results. Additionally, standard studies as done for R_K in Ref. [12] are also performed.

5.1 Systematic uncertainties for R_p

i) The COMPASS data taking was divided into periods, mainly depending upon the schedule of the SPS accelerator. A typical data period took about one week, and in between two periods interventions to the COMPASS spectrometer could happen. The whole 2006 data taking took about half a year. Therefore, it is verified that the values for R_p obtained from different data periods agree with one another.

ii) As in Ref. [12], and contrary to standard multiplicity analyses [9–11], two trigger types are used in this analysis, with or without the requirement of energy deposit in the calorimeters. It is verified that these two trigger types give consistent values for R_p. This result is expected as for the lowest proton energy analysed (20 GeV) calorimeter efficiencies are already close to 100%.

iii) The key correction factor that has to be applied to the raw value of R_p is the acceptance difference between p and $\bar{p}$. The COMPASS spectrometer is charge symmetric at the level of 1%. However, protons and anti-protons interact differently with the target material as they do not have the same re-interaction length in the long solid-state COMPASS ^{6}LiD target. Therefore, as already mentioned in Sect. 4, the acceptance for $\bar{p}$ is about 10% lower than that for p, with an estimated uncertainty of about 3%.

iv) More complex methods of unfolding the acceptance were tested in Ref. [12], as well as in the present analysis. They are giving very similar results when compared to the selected method, but their resulting covariance matrix has large off-diagonal elements. On the contrary, for the selected method the results in each bin and their statistical uncertainties can be considered to be independent from each other.

v) A correction factor has to be taken into account because of possibly different RICH reconstruction efficiencies for p and $\bar{p}$. While the correction factor is found to be one, the systematic studies suggest that its uncertainty is about 5%. This uncertainty on R_p is by 2% larger than that found for R_K, mostly due to the higher mass of the proton compared to that of the kaon, which leads to less photons per ring in the RICH in most of the phase space region covered. On top of that, some performed tests are limited in precision due to the small statistics, especially for anti-protons at larger momenta and/or larger values of z.

vi) As in previous studies, the stability of R_p is tested on data using several variables that are defined in the spectrometer coordinate system. A clear instability is seen in the dependence of R_p upon the azimuthal angle measured in the laboratory frame, as it was the case in our earlier analysis of R_K. In Ref. [12], this asymmetry led to a systematic uncertainty of up to 12% in both x-bins. In this analysis, for data binned in x and z, the systematic uncertainty amounts up to 5% for the 1st x-bin and up to 11% in the 2nd x-bin. For data binned in z and p_h, it can be up to 15% for high momenta. Thus in a significant part of the phase space this systematic uncertainty is the dominant one.

The total systematic uncertainty of R_p is obtained by adding in quadrature the above discussed contributions. The relative systematic uncertainty is found to range between 6% and 16%. The correlation between systematic uncertainties in various z and p_h-bins is about 0.7–0.8, as in Ref. [12].

5.2 Systematic uncertainties for R_K

Most studies of systematic effects for kaon results follow closely the ones from Ref. [12], which are also described above for protons. The systematic uncertainty related to the acceptance ratio and the RICH efficiency ratio for the two kaon charges is taken as in Ref. [12], *i.e.* 2% and 3%, respectively. The uncertainty related to the azimuthal-angle distribution of hadrons in the spectrometer is studied using the same method as in our previous paper and the resulting relative uncertainty ranges between 4% and 12%. Compared to the analysis presented in Ref. [12], a new type of systematic uncertainty has to be studied, which is related to the new method of extracting the raw kaon yields from RICH data.

First, it is verified that the results obtained with the new method do agree with those previously published [12]. Various combinations of functional forms are used in the fit, *e.g.* the main results are ob-

tained using a Gaussian functional form to fit the polar-angle distribution of the kaon and two Gaussian functions for the one of the pion. In the systematic studies, we use a single or two Gaussian function(s) for each particle type. With three Gaussian functions to describe the polar-angle distribution of photons in the RICH detector, there are nine free parameters in every single z and hadron momentum bin, and for each of the two hadron charges. The fit in certain bins (at large z and large momentum) results in very large uncertainties on the obtained values of $R_{\rm K}$. In order to improve accuracy, studies are performed to determine which parameters can be kept common for the two charges and across various z and momentum bins. For example, the pion and kaon Cherenkov opening angles depend only on the particle momenta but not on z. Indeed, it is confirmed in the fit that this angle is independent on z within uncertainties. Altogether, the initial 450 free parameters in the fit are reduced by about a factor of three. The systematic uncertainty of the final results on $R_{\rm K}$ is evaluated by performing several fits, in which the number of free parameters is reduced by releasing certain constraints.

As a systematic uncertainty, half of the difference between maximum and minimum value of $R_{\rm K}$ obtained in these studies is taken. The resulting relative uncertainty of the kaon yield is found to range between 4% and 25%. The total systematic uncertainty of $R_{\rm K}$ is found to range between 7% and 28% of the $R_{\rm K}$ value, and correspondingly between 0.4 and 1.1 of the statistical uncertainty on $R_{\rm K}$. As in previous analyses, the correlation between systematic uncertainties in various z and p_h-bins is about 0.7–0.8. We note that a fit of all data simultaneously may introduce correlations between $R_{\rm K}$ values in different z and p_h-bins. These correlations are found to be below 5% and hence neglected.

6 Results and discussion

In Fig. 2 and Table 1, the results on the anti-proton over proton multiplicity ratio $R_{\rm p}$ are presented as a function of the variable $z_{\rm corr}$ for the two x-bins used in this analysis. The measured z-dependence of $R_{\rm p}$ can be fitted in both x-bins by simple functional forms, *e.g.* $\propto (1-z)^{\beta}$. The obtained β value for this fit, $\beta = 0.75 \pm 0.04$, agrees within uncertainties well with $\beta = 0.71 \pm 0.03$ obtained from the fit to $R_{\rm K}$ in Ref. [12]. Presently, it is not clear if this observed agreement between kaons and protons is accidental or not. A "double ratio" $D_{\rm p} = R_{\rm p}(x < 0.05)/R_{\rm p}(x > 0.05)$, is shown in the insert of the figure. It may be considered constant within uncertainties over the full measured z-range, with an average value of $D_{\rm p} = 1.62 \pm 0.04_{\rm stat.} \pm 0.07_{\rm syst.}$.

The most important observation is that with the increase of z the measured value of $R_{\rm p}$ is increasingly undershooting the LO pQCD expectation, which is 0.51 and 0.28 calculated for the average kinematics of the data in the 1st and 2nd x-bin, respectively. It is remarkable that $R_{\rm p}$ falls below the LO pQCD prediction over the whole measured z range, which starts in this analysis from $z > 0.5$. This effect was observed for $R_{\rm K}$ only for $z > 0.8$. In Fig. 3, the comparison of $R_{\rm p}$ with $R_{\rm K}$ calculated using data in Ref. [10] and from Ref. [12] shows that over the whole measured phase space $R_{\rm p}$ falls significantly below $R_{\rm K}$. As mentioned above, the x and Q^2 distributions from the two analyses are different, which can change the results by about 5-10%. We hence avoid to quote precise results on the $R_{\rm p}/R_{\rm K}$ ratio here. As discussed in Section 2, the lower limit for $R_{\rm p}$ and $R_{\rm K}$ in LO pQCD is the same. For the ratio itself, a small difference of the order of 10% is expected due to the presence of favoured strange-quark fragmentation in the kaon case. The two effects, *i.e.* different x and Q^2 distributions and favoured strange quark fragmentation in the case of kaons, act in opposite directions. Thus in naive LO pQCD one would expect the proton and kaon data points shown in Fig. 3 to agree within better than 5%, which is clearly not the case. This indicates that the additional correction to the pQCD formalism we suggested in Ref. [12], which takes into account the phase space available for hadronisation, depends on the mass of the produced hadron.

One of the striking features of the observed disagreement between the expectation of (N)LO pQCD and the results on $R_{\rm K}$ obtained in Ref. [12] was the observed strong dependence of $R_{\rm K}$ on the virtual-photon

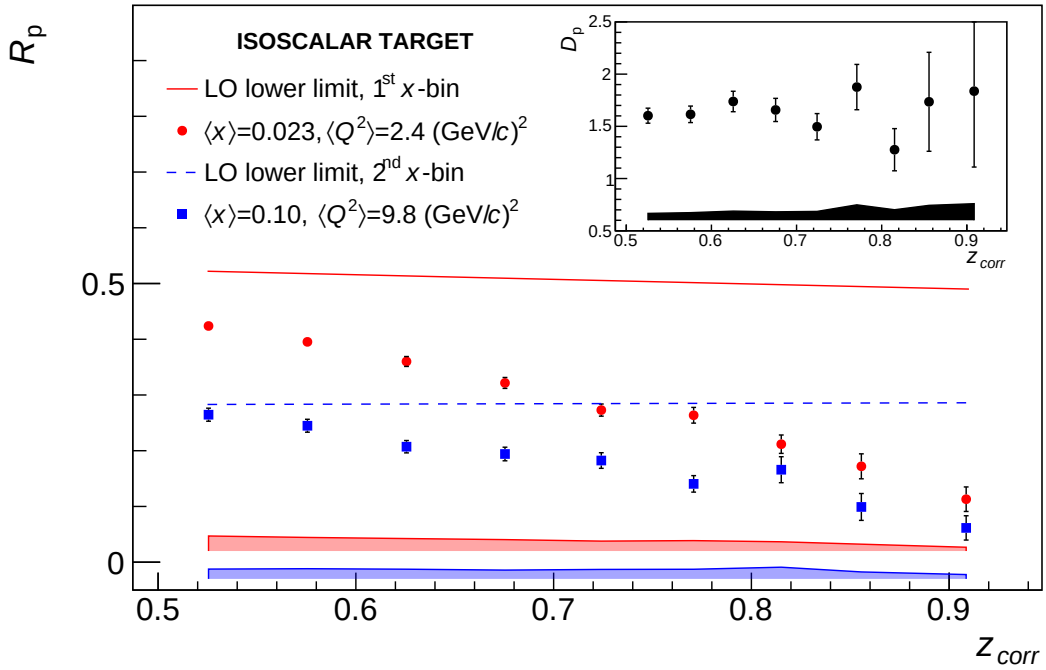

Fig. 2: Results on $R_{\rm p}$ as a function of $z_{\rm corr}$ for the two x-bins. The insert shows the double ratio $D_{\rm p}$ defined as the ratio of $R_{\rm p}$ in the first x-bin over $R_{\rm p}$ in the second x-bin. Statistical uncertainties are shown by error bars and systematic uncertainties by shaded bands at the bottom. The lines indicate the lower limit on $R_{\rm p}$ predicted by LO pQCD using the PDF set from Ref. [17]. The relative uncertainty of the limit is below 4% in both x-bins.

energy ν, with values of $R_{\rm K}$ closer to the pQCD prediction for higher ν. Our present results on $R_{\rm p}$ do confirm a similar dependence for the proton case. These results as well as the prediction of LO pQCD are shown in Fig. 4 and in Table 2. Much higher energies than those available in COMPASS seem to be required to eventually reach in the high-z region the lower limit of $R_{\rm p}$ predicted by LO pQCD. We mention that the lower limit of $R_{\rm p}$ does not directly depend on ν. The ν-dependence of the pQCD lower limit seen in Fig. 4 is related to different mean values of x and Q^2 for different values of ν.

In Ref. [12] it was found that the z and ν dependences, which are both unexpected in pQCD, can be combined in the dependence on only one observable, which is the missing mass in the final state that is approximately given by $M_X = \sqrt{M_{\rm p}^2 + 2M_{\rm p}\nu(1-z) - Q^2(1-z)^2}$. In Fig. 5 the antiproton over proton multiplicity ratio $R_{\rm p}$ is shown as a function of the missing mass, and indeed a smooth trend with overlapping points at different values of z is observed.

The strong ν dependence of $R_{\rm K}$ discussed above, as originally seen in Ref. [12], was also the inspiration to extend the covered ν range by improving the RICH K-π separation. In this way, kaon identification up to 55 GeV/c was achieved instead of 40 GeV/c previously, which allows us to extend the covered ν range in every z bin. In Fig. 6, the obtained results of $R_{\rm K}$ in bins of z as a function of ν in the extended momentum range are compared to the ones published in Ref. [12], as well as to the NLO pQCD lower limit for $R_{\rm K}$. The results confirm that the compatibility with pQCD expectations is better at higher ν. They also suggest that with increasing values of ν the growth of the ratio $R_{\rm K}$ becomes smaller. These results are also given in Table 3.

For completeness, in Fig. 7 the values of $R_{\rm K}$ in the extended momentum range are compared to our earlier results [12] as a function of missing mass. The smooth growth with M_X is still seen over the full kinematically accessible range. Now there is larger overlap in M_X between different z-bins, *i.e.* one can find M_X regions where in four different z bins at very different values of ν the results on $R_{\rm K}$ are found to

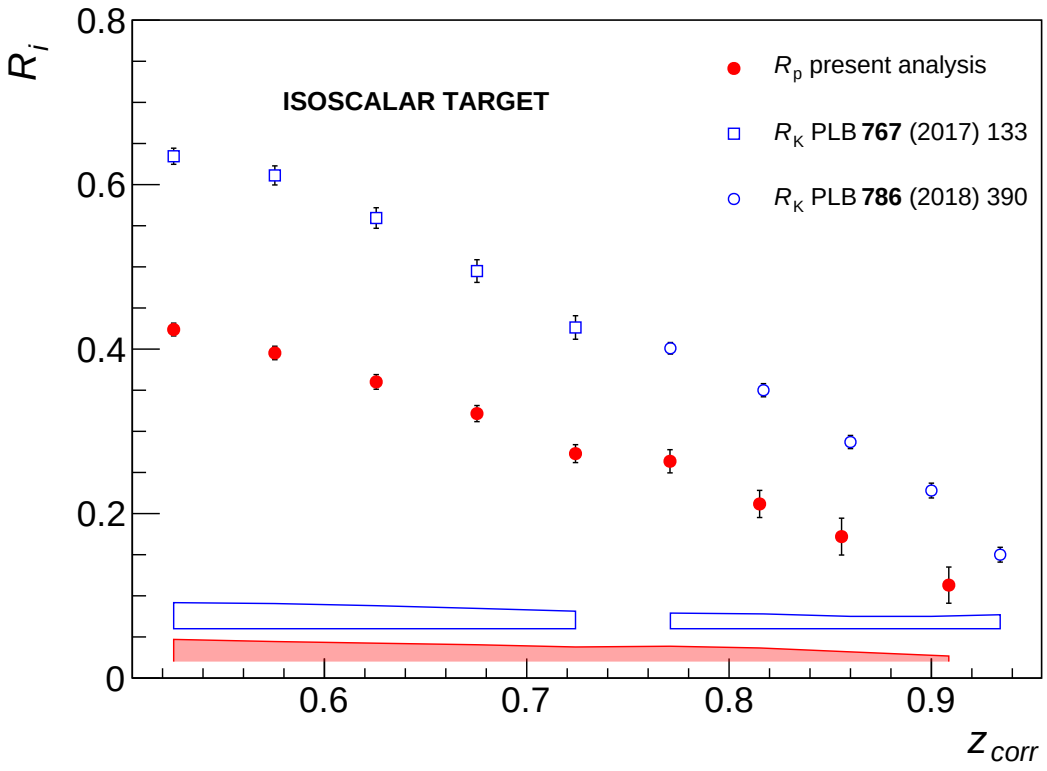

Fig. 3: Results on R_p and R_K as a function of z_{corr} for the first x-bin, $x < 0.05$. The ratio R_p falls below R_K in the whole measured phase space. The kaon data come from Refs. [10, 12]. Statistical uncertainties are shown by error bars, systematic uncertainties by the bands at the bottom.

be consistent with one another.

7 Summary

In this article the $\bar{p}$ over p multiplicity ratio R_p, obtained from semi-inclusive measurements of deep-inelastic lepton-nucleon scattering at z-values above 0.5, is presented for the first time. In the whole studied z-region the ratio R_p is observed to be below the lower limit predicted by LO pQCD. It is found to be significantly smaller than the K^- over K^+ multiplicity ratio R_K as presented in our previous letter, while in naive LO pQCD both ratios are expected to be very similar. A strong dependence on the virtual-photon energy ν is observed, which is also not expected by LO pQCD but was already seen for the ratio R_K in our earlier analysis. In this article, the analysis of R_K is extended to larger values of ν up to 70 GeV. The obtained results suggest that for high ν values there is an indication for saturation of R_K at or above the value predicted by NLO pQCD. The present studies provide further support that the additional correction to the pQCD formalism suggested in our previous paper, which takes into account the phase space available for hadronisation, depends on the mass of the produced hadron.

Acknowledgements

We gratefully acknowledge the support of the CERN management and staff and the skill and effort of the technicians of our collaborating institutes. This work was made possible by the financial support of our funding agencies.

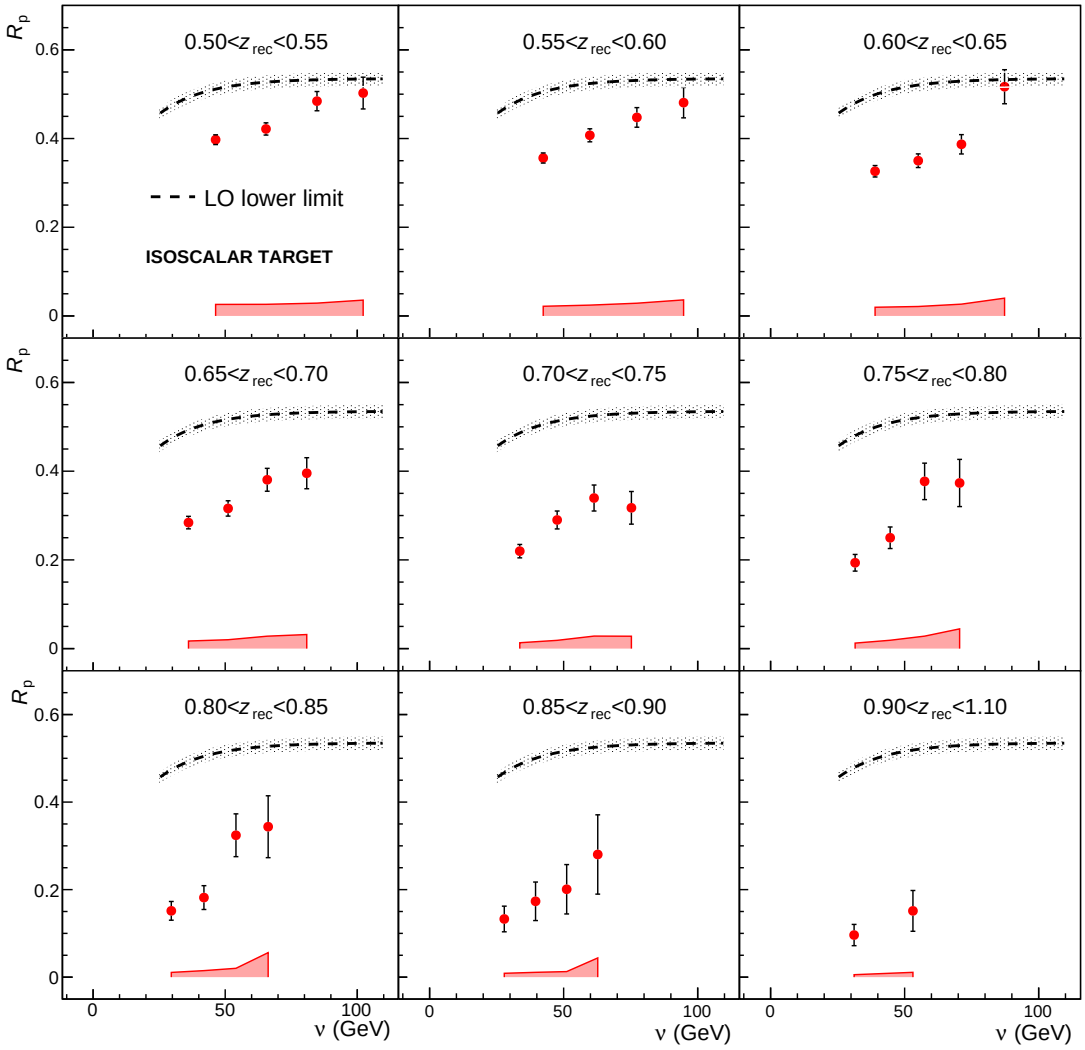

Fig. 4: Results on $R_{\rm p}$ as a function of ν in nine bins of $z_{\rm rec}$ for the first x-bin, $x < 0.05$. Statistical uncertainties are shown by error bars, systematic uncertainties by the shaded bands at the bottom. The curves represent the lower limits for $R_{\rm p}$ calculated in LO pQCD using [17] PDF set. The shaded bands around the LO lower limits indicates their uncertainty.

References

[1] V.N. Gribov and L.N. Lipatov, Sov. J. Nucl. Phys. **15** (1972) 438; L.N. Lipatov, *ibid.* **20** (1975) 95; G. Altarelli and G. Parisi, Nucl. Phys. B **126** (1977) 298; Yu.L. Dokshitzer, Sov. Phys. JETP **46** (1977) 641.

[2] M. Hirai, S. Kumano, T.-H. Nagai and K. Sudoh, Phys. Rev. D **75** (2007) 094009.

[3] M. Hirai, H. Kawamura, S. Kumano and K. Saito, Prog. Theor. Exp. Phys. **2016** (2016) 113B04.

[4] N. Sato *et al.*, Phys. Rev. D **94** (2016) 114004.

[5] D. de Florian, R. Sassot and M. Stratmann, Phys. Rev. D **75** (2007) 114010.

[6] D. de Florian *et al.*, Phys. Rev. D **95** (2017) 094019.

[7] NNPDF Collaboration, V. Bertone *et al.*, Eur. Phys. J. C **77** (2017) 516.

[8] HERMES Collaboration, A. Airapetian *et al.*, Phys. Rev. D **87** (2013) 074029.

[9] COMPASS Collaboration, C. Adolph *et al.*, Phys. Lett. B **764** (2017) 1.

[10] COMPASS Collaboration, C. Adolph *et al.*, Phys. Lett. B **767** (2017) 133.

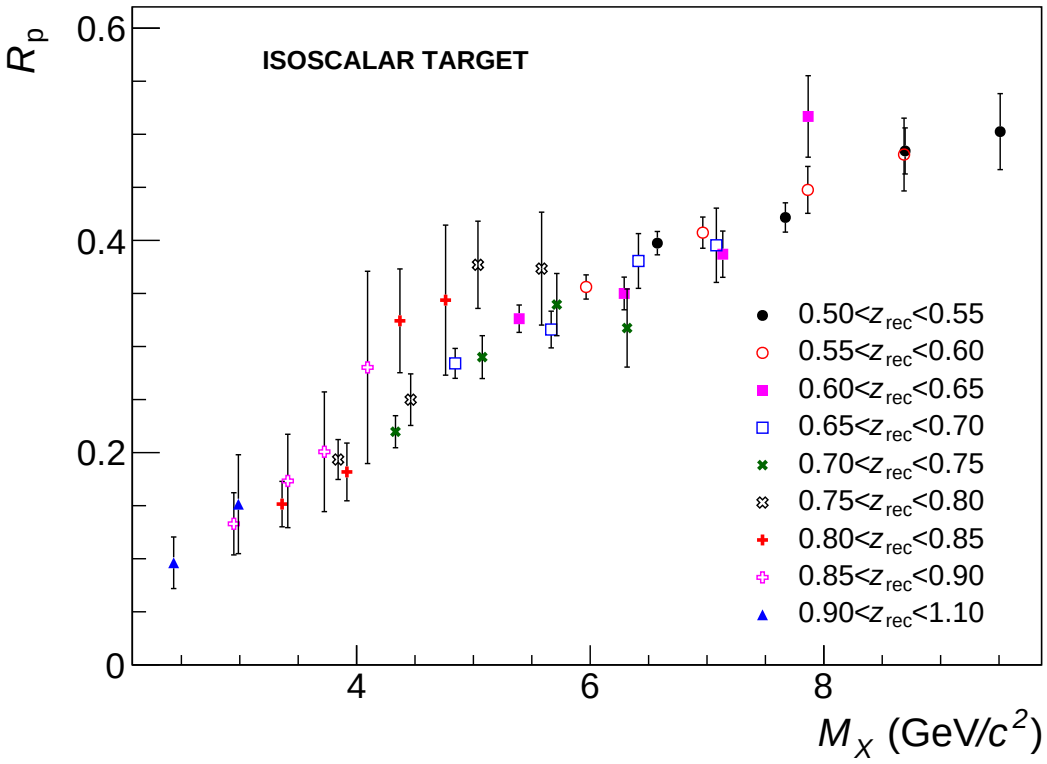

Fig. 5: Results on R_p as a function of missing mass M_X for the first x-bin, $x < 0.05$. For clarity only statistical uncertainties are shown.

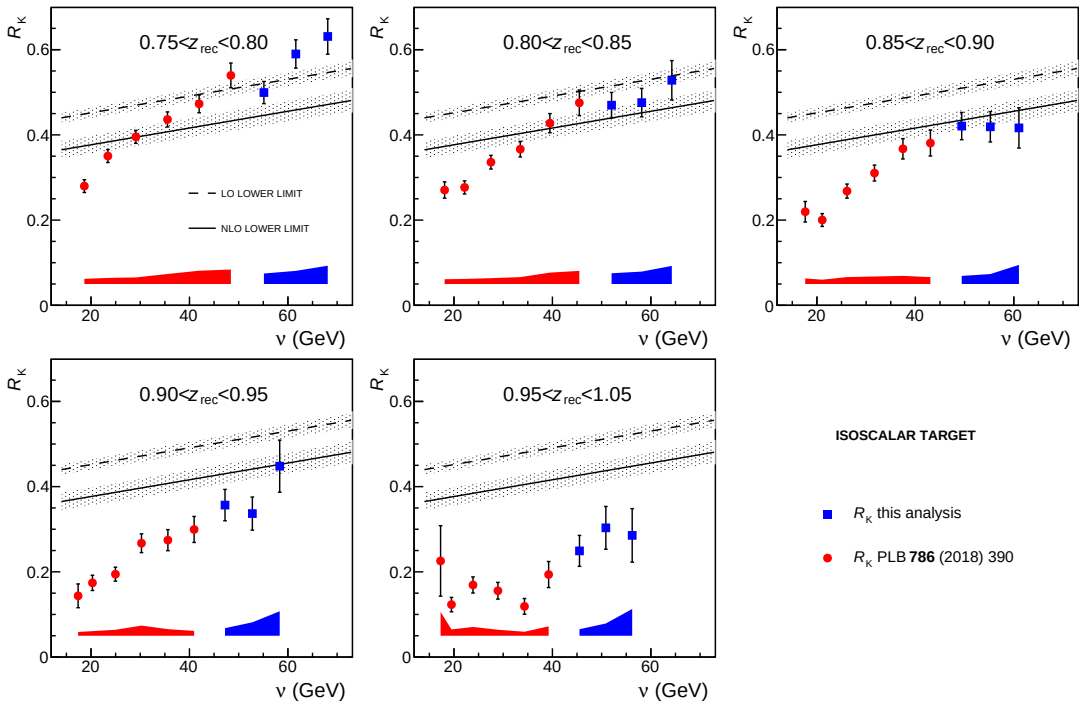

Fig. 6: The K^- over K^+ multiplicity ratio as a function of ν in five bins of z obtained in this analysis (blue) and in Ref. [12] (red). The errors bars represent statistical uncertainties. The systematic uncertainties of the data points are indicated by the shaded band at the bottom of each panel. The shaded bands around the (N)LO lower limits indicate their uncertainties.

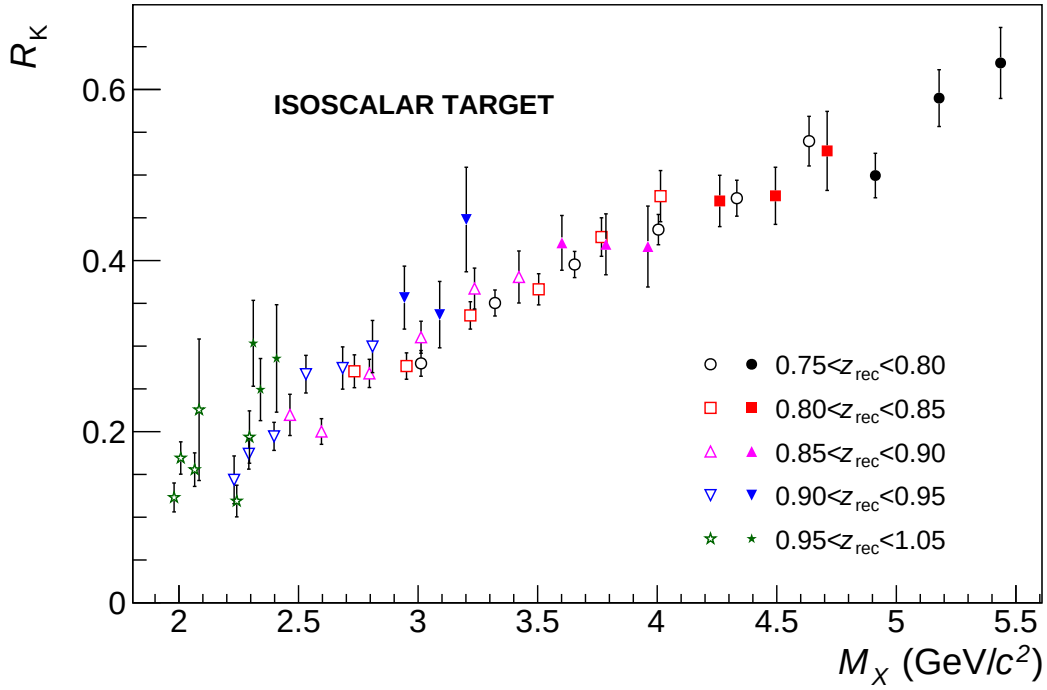

Fig. 7: The K^- over K^+ multiplicity ratio presented as a function of M_X for this analysis (full symbols) and for the analysis in Ref. [12] (open symbols), see text for details. For clarity only statistical uncertainties are shown.

[11] COMPASS Collaboration, M. Aghasyan *et al.*, Phys. Rev. D **97** (2018) 032006.
[12] COMPASS Collaboration, R. Akhunzyanov *et al.*, Phys. Lett. B **786** (2018) 390.
[13] M. Anselmino *et al.*, Phys. Rev. D **71** (2005) 074006.
[14] W. Furmanski and R. Petronzio, Z. Phys. C **11** (1982) 293.
[15] D. de Florian, M. Stratmann and W. Vogelsang, Phys. Rev. D **57** (1998) 5811.
[16] R. Jakob, P. J. Mulders and J. Rodrigues, Nucl. Phys. A **626** (1997) 937.
[17] A. D. Martin, W. J. Stirling, R. S. Thorne and G. Watt, Eur. Phys. J. C **64** (2009) 653.
[18] L. A. Harland-Lang, A. D. Martin, P. Motylinski and R. S. Thorne, Eur. Phys. J. C **75** (2015) 204.
[19] NNPDF Collaboration, R. D. Ball *et al.*, J. High En. Phys. **04** (2015) 040.
[20] G. Ingelman, A. Edin and J. Rathsman, Comput. Phys. Commun. **101** (1997) 108.
[21] T. Sjöstrand, LU-TP-95-20, CERN-TH-7112-93-REV, hep-ph/9508391.
[22] A. Kotzinian, Eur. Phys. J. C **44** (2005) 211.
[23] J. V. Guerrero *et al.*, J. High En. Phys. **09** (2015) 169.
[24] E. Christova and E. Leader, Phys. Rev. D **94** (2016) 096001.
[25] J. V. Guerrero and A. Accardi, Phys. Rev. D **97** (2018) 114012.
[26] D. P. Anderle, F. Ringer and W. Vogelsang, Phys. Rev. D **87** (2013) 034014.
[27] D. P. Anderle, M. Stratmann and F. Ringer, Phys. Rev. D **92** (2015) 114017.
[28] D. P. Anderle, T. Kaufmann, M. Stratmann and F. Ringer, Phys. Rev. D **95** (2017) 054003.
[29] M. Epele, C. G. Canal and R. Sassot, Phys. Rev. D **94** (2016) 034037.
[30] M. Epele, C. G. Canal and R. Sassot, Phys. Lett. B **790** (2019) 102.
[31] A. Accardi and A. Signori, Phys. Lett. B **798** (2019) 134993.
[32] COMPASS Collaboration, P. Abbon *et al.*, Nucl. Instr. and Meth. A **577** (2007) 455.
[33] P. Abbon *et al.*, Nucl. Instr. and Meth. A **631** (2011) 26.
[34] E. C. Aschenauer *et al.*, Phys. Rev. D **88** (2013) 114025; H. Spiesberger, HERACLES and DJAN-

Table 1: Extracted values of R_p with statistical and systematic uncertainties, bin limits of z (z_{min}, z_{max}), and average values of x, Q^2, z_{rec} and z_{corr} in the first (upper part) and second (lower part) x-bin.

bin	x	Q^2 (GeV/c)^2	z_{min}	z_{max}	z_{rec}	z_{corr}	$R_p \pm \delta R_{p,stat.} \pm \delta R_{p,syst.}$
1	0.021	2.4	0.50	0.55	0.524	0.524	$0.4238 \pm 0.0078 \pm 0.0270$
2	0.022	2.2	0.55	0.60	0.575	0.575	$0.3953 \pm 0.0082 \pm 0.0244$
3	0.022	2.1	0.60	0.65	0.624	0.624	$0.3601 \pm 0.0089 \pm 0.0224$
4	0.023	2.0	0.65	0.70	0.675	0.675	$0.3216 \pm 0.0098 \pm 0.0205$
5	0.024	1.9	0.70	0.75	0.724	0.724	$0.2729 \pm 0.0109 \pm 0.0178$
6	0.025	1.8	0.75	0.80	0.775	0.774	$0.2636 \pm 0.0141 \pm 0.0187$
7	0.026	1.8	0.80	0.85	0.826	0.820	$0.2117 \pm 0.0165 \pm 0.0166$
8	0.026	1.7	0.85	0.90	0.878	0.865	$0.1720 \pm 0.0224 \pm 0.0123$
9	0.028	1.7	0.90	1.10	0.948	0.915	$0.1130 \pm 0.0220 \pm 0.0068$
1’	0.100	10.5	0.50	0.55	0.525	0.525	$0.2646 \pm 0.0117 \pm 0.0176$
2’	0.101	9.7	0.55	0.60	0.575	0.575	$0.2448 \pm 0.0116 \pm 0.0183$
3’	0.101	9.0	0.60	0.65	0.625	0.625	$0.2072 \pm 0.0111 \pm 0.0174$
4’	0.101	8.4	0.65	0.70	0.675	0.675	$0.1941 \pm 0.0122 \pm 0.0158$
5’	0.100	7.8	0.70	0.75	0.725	0.725	$0.1824 \pm 0.0140 \pm 0.0170$
6’	0.102	7.5	0.75	0.80	0.774	0.771	$0.1405 \pm 0.0148 \pm 0.0173$
7’	0.102	7.1	0.80	0.85	0.823	0.815	$0.1659 \pm 0.0233 \pm 0.0210$
8’	0.099	6.4	0.85	0.90	0.872	0.855	$0.0991 \pm 0.0241 \pm 0.0125$
9’	0.104	5.9	0.90	1.10	0.948	0.910	$0.0615 \pm 0.0218 \pm 0.0078$

GOH : Event Generation of ep Interactions at HERA Including Radiative Processes (version 1.6).

Table 2: Extracted values of R_{p} with statistical and systematic uncertainties, bin range of proton momenta (p_{rg} (GeV/c)), bin range in z (z_{rg}), and average values of x, Q^2, z_{rec} and z_{corr} in the first x-bin.

bin	x	Q^2 (GeV/c)^2	p_{rg} (GeV/c)	z_{rg}	z_{rec}	z_{corr}	$R_{\mathrm{p}} \pm \delta R_{\mathrm{p,stat.}} \pm \delta R_{\mathrm{p,syst.}}$
1a	0.022	1.9	20–30	0.50–0.55	0.524	0.524	$0.3973 \pm 0.0110 \pm 0.0260$
1b	0.020	2.5	30–40	0.50–0.55	0.525	0.525	$0.4215 \pm 0.0138 \pm 0.0262$
1c	0.020	3.2	40–50	0.50–0.55	0.524	0.524	$0.4843 \pm 0.0217 \pm 0.0289$
1d	0.021	4.0	50–60	0.50–0.55	0.526	0.526	$0.5024 \pm 0.0358 \pm 0.0357$
2a	0.023	1.9	20–30	0.55–0.60	0.575	0.575	$0.3561 \pm 0.0114 \pm 0.0218$
2b	0.020	2.3	30–40	0.55–0.60	0.574	0.574	$0.4073 \pm 0.0147 \pm 0.0244$
2c	0.020	3.0	40–50	0.55–0.60	0.575	0.575	$0.4476 \pm 0.0221 \pm 0.0287$
2d	0.020	3.6	50–60	0.55–0.60	0.575	0.575	$0.4808 \pm 0.0343 \pm 0.0362$
3a	0.024	1.8	20–30	0.60–0.65	0.624	0.624	$0.3262 \pm 0.0129 \pm 0.0196$
3b	0.021	2.1	30–40	0.60–0.65	0.625	0.625	$0.3499 \pm 0.0154 \pm 0.0213$
3c	0.020	2.7	40–50	0.60–0.65	0.624	0.624	$0.3870 \pm 0.0218 \pm 0.0266$
3d	0.020	3.3	50–60	0.60–0.65	0.624	0.624	$0.5167 \pm 0.0384 \pm 0.0401$
4a	0.026	1.7	20–30	0.65–0.70	0.675	0.675	$0.2840 \pm 0.0141 \pm 0.0171$
4b	0.021	2.0	30–40	0.65–0.70	0.675	0.675	$0.3160 \pm 0.0173 \pm 0.0200$
4c	0.020	2.5	40–50	0.65–0.70	0.675	0.675	$0.3806 \pm 0.0258 \pm 0.0280$
4d	0.020	3.1	50–60	0.65–0.70	0.675	0.675	$0.3954 \pm 0.0350 \pm 0.0317$
5a	0.027	1.7	20–30	0.70–0.75	0.724	0.724	$0.2197 \pm 0.0151 \pm 0.0132$
5b	0.022	1.9	30–40	0.70–0.75	0.724	0.724	$0.2899 \pm 0.0202 \pm 0.0186$
5c	0.020	2.3	40–50	0.70–0.75	0.725	0.725	$0.3395 \pm 0.0293 \pm 0.0282$
5d	0.020	2.9	50–60	0.70–0.75	0.724	0.724	$0.3174 \pm 0.0368 \pm 0.0279$
6a	0.028	1.6	20–30	0.75–0.80	0.776	0.773	$0.1935 \pm 0.0188 \pm 0.0124$
6b	0.022	1.9	30–40	0.75–0.80	0.775	0.774	$0.2499 \pm 0.0243 \pm 0.0188$
6c	0.020	2.2	40–50	0.75–0.80	0.774	0.774	$0.3770 \pm 0.0411 \pm 0.0281$
6d	0.020	2.7	50–60	0.75–0.80	0.774	0.773	$0.3734 \pm 0.0532 \pm 0.0445$
7a	0.029	1.6	20–30	0.80–0.85	0.827	0.819	$0.1515 \pm 0.0214 \pm 0.0108$
7b	0.023	1.8	30–40	0.80–0.85	0.824	0.819	$0.1818 \pm 0.0272 \pm 0.0149$
7c	0.020	2.1	40–50	0.80–0.85	0.824	0.821	$0.3242 \pm 0.0489 \pm 0.0202$
7d	0.020	2.5	50–60	0.80–0.85	0.823	0.820	$0.3437 \pm 0.0707 \pm 0.0560$
8a	0.030	1.5	20–30	0.85–0.90	0.882	0.866	$0.1329 \pm 0.0293 \pm 0.0088$
8b	0.024	1.8	30–40	0.85–0.90	0.875	0.862	$0.1733 \pm 0.0440 \pm 0.0124$
8c	0.020	2.0	40–50	0.85–0.90	0.874	0.865	$0.2008 \pm 0.0564 \pm 0.0127$
8d	0.020	2.3	50–60	0.85–0.90	0.872	0.865	$0.2802 \pm 0.0906 \pm 0.0437$
9ab	0.031	1.5	20–40	0.90–1.10	0.954	0.917	$0.0958 \pm 0.0242 \pm 0.0057$
9cd	0.022	2.0	40–60	0.90–1.10	0.936	0.910	$0.1466 \pm 0.0451 \pm 0.0099$

Table 3: Extracted values of R_{K} with statistical and systematic uncertainties, bin range of kaon momenta (p_{rg} (GeV/c)), bin range in z (z_{rg}), and average values of x, Q^2, z_{rec} and z_{corr}.

bin	x	Q^2 (GeV/c)^2	p_{rg} (GeV/c)	z_{rg}	z_{rec}	z_{corr}	$R_{\mathrm{K}} \pm \delta R_{\mathrm{K,\,stat.}} \pm \delta R_{\mathrm{K,\,syst.}}$
1g	0.021	2.1	40–45	0.75–0.80	0.774	0.774	$0.4994 \pm 0.0260 \pm 0.0246$
1h	0.020	2.3	45–50	0.75–0.80	0.774	0.774	$0.5899 \pm 0.0332 \pm 0.0308$
1i	0.019	2.4	50–55	0.75–0.80	0.774	0.774	$0.6310 \pm 0.0415 \pm 0.0429$
2g	0.022	2.1	40–45	0.80–0.85	0.824	0.822	$0.4697 \pm 0.0300 \pm 0.0252$
2h	0.020	2.2	45–50	0.80–0.85	0.823	0.822	$0.4757 \pm 0.0334 \pm 0.0291$
2i	0.019	2.3	50–55	0.80–0.85	0.823	0.822	$0.5282 \pm 0.0462 \pm 0.0425$
3g	0.022	2.0	40–45	0.85–0.90	0.872	0.868	$0.4207 \pm 0.0320 \pm 0.0190$
3h	0.021	2.1	45–50	0.85–0.90	0.873	0.869	$0.4190 \pm 0.0356 \pm 0.0233$
3i	0.020	2.2	50–55	0.85–0.90	0.872	0.869	$0.4164 \pm 0.0473 \pm 0.0448$
4g	0.022	1.9	40–45	0.90–0.95	0.921	0.911	$0.3567 \pm 0.0368 \pm 0.0178$
4h	0.021	2.1	45–50	0.90–0.95	0.921	0.911	$0.3368 \pm 0.0388 \pm 0.0315$
4i	0.020	2.2	50–55	0.90–0.95	0.921	0.913	$0.4480 \pm 0.0611 \pm 0.0575$
5g	0.023	1.9	40–45	0.95–1.05	0.974	0.945	$0.2492 \pm 0.0363 \pm 0.0153$
5h	0.022	2.0	45–50	0.95–1.05	0.975	0.952	$0.3033 \pm 0.0502 \pm 0.0288$
5i	0.020	2.1	50–55	0.95–1.05	0.974	0.952	$0.2856 \pm 0.0628 \pm 0.0628$